1st Symposium on Advances in Approximate Bayesian Inference, 2018 1–8

Approximate Bayesian inference for robotic mapping

Anthony Tompkins * ANTHONY.TOMPKINS@SYDNEY.EDU.AU
Ransalu Senanayake RANSALU.SENANAYAKE@SYDNEY.EDU.AU
Fabio Ramos FABIO.RAMOS@SYDNEY.EDU.AU
School of Computer Science, The University of Sydney, Australia

Abstract

In order to deploy robots in previously unseen and unstructured environments, the robots should have the capacity to learn on their own and adapt to the changes in the environments. For instance, in mobile robotics, a robot should be able to learn a map of the environment from data itself without the intervention of a human to tune the parameters of the model. However, often time, learning parameters of the map model is challenging because the models of the maps are specified as Bayesian models with intractable posterior distributions. In this paper, we evaluate the use of variational inference with the *reparameterization trick* to learn parameters of the map model using *probabilistic programming*. We demonstrate that the model learns tens of thousands of parameters within minutes in both big data and data-scarce regimes.

1. Introduction

In the era of self-driving cars, modeling the uncertainties of the environment a robot operates in is crucial to safer decision-making. To this end, discerning occupied areas from unoccupied areas of the environment using depth sensor measurements such as LiDAR is required. Typically, these occupancy states exhibit highly nonlinear and spatially correlated patterns that cannot be captured with a simple linear classification model. Therefore, kernel methods have been the *de jure* choice in recent occupancy mapping (Ramos and Ott, 2015; Doherty et al., 2016). Further, experiments have corroborated their promising applications in 2D, 3D, and spatiotemporal mapping (Doherty et al., 2016), though with some heuristic parameter choices.

One of the recent methods for occupancy mapping is Bayesian Hilbert maps (BHMs) (Senanayake and Ramos, 2017) which is a robust extension to Hilbert Maps (Ramos and Ott, 2015). In BHMs, the map is learned on a reproducing kernel Hilbert space (RKHS) where kernel functions are used to characterize spatial relationships. A kernel $k(\mathbf{x}, \tilde{\mathbf{x}}) : \mathcal{X} \times \mathcal{X} \to \mathbb{R}$ is a function that measures the similarity between two multidimensional inputs $\mathbf{x}$, $\tilde{\mathbf{x}} \in \mathcal{X} \subset \mathbb{R}^2$. In mapping, the pairwise similarities between the elements of the two sets of points $\{\mathbf{x}_n \in \mathbb{R}^2\}_{n=1}^N$ and $\{\tilde{\mathbf{x}}_m \in \mathbb{R}^2\}_{m=1}^M$ are computed. Here, $\mathbf{x}$ are longitude-latitude locations of either free or occupied $y \in \{0, 1\} = \{\text{free}, \text{occupied}\}$ data points sampled from laser beams and $\tilde{\mathbf{x}}$ are points *anchored* on pre-defined locations of the space. A squared-exponential (SE) kernel $k(\mathbf{x}_n, \tilde{\mathbf{x}}_m; l) = \exp\big(-\|\mathbf{x}_n - \tilde{\mathbf{x}}_m\|_2^2 / 2l^2\big)$

* This paper is an extension to Senanayake et al. (2018)

with a heuristically determined lengthscale l is used to compute the the feature vector $\phi(\mathbf{x}_n; l) = (k(\mathbf{x}_n, \tilde{\mathbf{x}}_1; l), k(\mathbf{x}_n, \tilde{\mathbf{x}}_2; l), ..., k(\mathbf{x}_n, \tilde{\mathbf{x}}_M; l)) \in \mathbb{R}^{M\times 1}$ for all data points $\{\mathbf{x}_n\}_{n=1}^N$. In this sense, $\{(\mathbf{x}_n, y_n)\}_{n=1}^N$ is the dataset and $\left\{l, \{\tilde{\mathbf{x}}_m\}_{m=1}^M\right\}$ is the pre-defined parameter set.

Once the feature vector is evaluated, it passes through a sigmoidal function to estimate the occupancy level $\hat{y} = p(y|\mathbf{x}_*, \mathbf{w}) = 1/(1 + \exp(\mathbf{w}^\top \phi(\mathbf{x}_*; l)))$ of a query point in the space $\mathbf{x}_*$, given the weights $\mathbf{w}$. As this query point can be any longitude-latitude pair, BHMs can produce maps with arbitrary resolution at prediction time. One of the major challenges in employing kernel methods in occupancy mapping is the requirement of choosing parameters and hyperparameters of the model (Senanayake and Ramos, 2017). In order for mobile robots to maneuver fully autonomously in unknown environments or to interact with humans and other agents, the robots should have the capability to automatically learn their model parameters from data. This is further challenging since the parameters are spatially dependent - e.g. walls and furniture may contribute to sharp features while open spaces and large hills may contribute to spatially smooth features. The importance of nonstationarity is demonstrated in Figure 3 of the supplementary materials. In our contribution, we learn where to place kernels and what lengthscales they should have by introducing prior distributions over them. These autodidactic and model adaptation paradigms are vital for a robot to achieve full autonomy.

2. Model

We propose a method capable of learning both the shapes $\{l_m\}_{m=1}^M$ of the kernel and its longitude-latitude locations $\{\tilde{\mathbf{x}}_m = (\tilde{x}_m^{\text{lon}}, \tilde{x}_m^{\text{lat}})\}_{m=1}^M$ alongside feature weights $\{w_m\}_{m=1}^M$. Note that each kernel has its own lengthscale and location, and priors are introduced as in Figure 1 and Table 1. Our objective is to learn the posterior distribution. Because of the Bernoulli likelihood, the posterior is intractable and hence is approximated using another distribution q. The basic formulation with mean-field variational approximation is given in Figure 4 and the following equation,

$$\underbrace{\prod_{m=1}^{M} q(w_m)q(\mathbf{l}_m)q(\tilde{x}_m^{\text{lon}})q(\tilde{x}_m^{\text{lat}})}_{\text{factorized variational distribution}} = \underbrace{q(\mathbf{w}, \mathbf{l}, \tilde{\mathbf{x}})}_{\substack{\text{variational}\\ \text{distribution}}} \approx \underbrace{p(\mathbf{w}, \mathbf{l}, \tilde{\mathbf{x}}|\mathbf{x}, \mathbf{y})}_{\text{posterior}} \propto \underbrace{p(\mathbf{w})p(\mathbf{l})p(\tilde{\mathbf{x}})}_{\text{priors}} \underbrace{p(\mathbf{y}|\mathbf{x}, \mathbf{w}, \mathbf{l}, \tilde{\mathbf{x}})}_{\text{likelihood}}.$$

In essence, this is Bayesian logistic regression augmented with kernel features. However, this posterior distribution is intractable due to the Bernoulli likelihood. Since distributions over lengthscales and positions are introduced in addition to distributions over weights, obtaining a maximum a posteriori estimation is not feasible even with the lower bound derived in Jaakkola and Jordan (1997). As occupancy mapping is a very high dimensional problem, obtaining the posterior using Markov chain Monte Carlo techniques such as Hamiltonian Monte Carlo (Neal, 1993) is costly (Bishop, 2007). As an alternative, we use variational inference (VI) with the reparameterization trick (Kingma and Welling, 2013). Although there are other alternatives such as Black Box Variational Inference (Paisley et al., 2012; Ranganath et al., 2014; Mnih and Gregor, 2014), we used the well-established reparameterized variational inference (RVI) which is commonly used for variational autoencoders (Kingma and Welling, 2013) because it can easily perform stochastic gradient descent (SGD) with

minibatches for our model. In order to improve the expressive power of the model, Burda et al. (2015) proposed importance weighted variational inference (IWVI) which considers the weighted average of k approximate posterior samples. This induces a tighter log-likelihood lower bound. We made use of probabilistic programming (Tran et al., 2017) to minimize the Kullback-Leibler divergence between the variational distribution and posterior $\mathbb{KL}(q\|p)$.

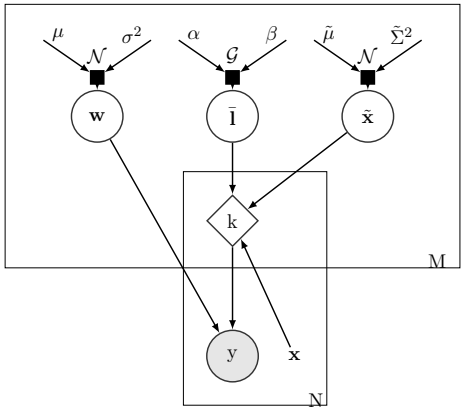

Figure 1: The graphical model. The kernel k is evaluated $N \times M$ times.

Table 1: Description of model parameters. Assuming independence, individual distributions are associated with all hinge points $m = 1...M$

Var.	Distributions
Prior distributions:	
w_m	$\mathcal{N}(\mu_m, \sigma_m^2)$ - Gaussian
$\bar{l}_m$	$\mathcal{G}(\alpha_m, \beta_m)$ - Gamma
$\tilde{\mathbf{x}}_m$	$\mathcal{N}(\tilde{\mu}, \tilde{\Sigma}^2)$
Variational distributions:	
qw_m	$\mathcal{N}(\mu_m^{(q)}, \sigma_m^{2(q)})$
$q\bar{l}_m$	$\mathcal{LN}(\alpha_m^{(q)}, \beta_m^{(q)})$ - Log-normal
$q\tilde{\mathbf{x}}_m$	$\mathcal{N}(\tilde{\mu}^{(q)}, \tilde{\sigma}^{2(q)})$

3. Experiments

We conducted experiments on four different datasets given in Table 3 given in Appendix C. These datasets contain both static and dynamic environments. As with Senanayake and Ramos (2017), our model will estimate the average long-term occupancy which is different from removing dynamics to build a static occupancy map (Meyer-Delius et al., 2012; Stachniss and Burgard, 2005). We also compared the proposed model, automorphing Bayesian Hilbert maps (ABHM) with RVI and IWVI, against variational sparse dynamic Gaussian process occupancy maps (VSDGPOM) (Senanayake et al., 2017) which utilizes stochastic variational inference with sparse Gaussian processes (Hensman et al., 2013). Model parameters were initialized randomly. The code is available online: `https://github.com/MushroomHunting/automorphing-kernels`.

This experiment was designed to validate the main contribution of the method—learning lengthscales and hinge locations. To understand the full effect of the proposed model it is not enough to look at the predicted occupancy map—we must consider the underlying distributions. Figure 2 provides a visual map of the means and variances of a learned model's variational posteriors. Accounting for a large part of the upper and lower parts of the map, the position variance in Figure 2b shows that in areas of dense laser scans where no walls exist, a larger but uniform variance for each spatial dimension is learned. For the areas where the laser scanner has detected walls one observes a stark contrast exhibited by the smaller spatial variances. In the walled area spanning the middle of the map the learned variances in the latitudinal direction are stretched out further relative to the longitudinal direction reflecting the narrow corridor-like shape of the wall. Concerning now the lengthscale mean and variance in Figure 2c we can observe the most significant effect in terms of the learned posteriors. At the top and the bottom open areas the largest lengthscales are observed

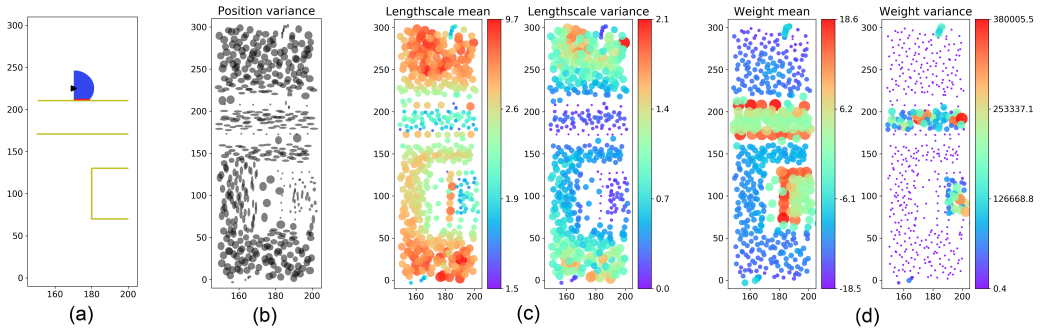

Figure 2: Uncertainty plots (a) A portion of the environment (b) Positions of hinge kernels $\tilde{\mathbf{x}}$ (c) Lengthscales (d) Weights

Table 2: Losses on all real datasets. The higher the area under curve (AUC) or the lower the mean negative log loss (MNLL), the better the model is.

Method	Dataset 1		Dataset 2		Dataset 3		Dataset 4	
	AUC	MNLL	AUC	MNLL	AUC	MNLL	AUC	MNLL
ABHM-RVI	**0.999**	**0.015**	**0.994**	**0.093**	**0.993**	**0.175**	**0.889**	**0.477**
ABHM-IWRVI	0.980	0.192	0.994	0.660	0.988	0.227	0.864	0.525
BHM	**1.000**	0.176	0.921	0.362	0.990	0.280	0.825	0.570
HM	0.992	0.226	0.938	0.666	0.920	0.903	0.778	0.677
VSDGPOM	0.801	0.372	0.794	0.530	0.990	0.233	0.788	0.886
DOGM	0.792	0.593	0.901	0.744	0.980	0.495	0.779	3.449

signifying a minimal complexity of occupancy. Paralleling the learned position variances, the learned lengthscale means are clustered around either areas of detail or areas of uncertain occupancy. This effect is repeated in the lengthscale variance and we observe similar effects across kernel weight means and variances in Figure 2d. This underlying analysis of the learned posterior distributions not only substantiates the motivation for spatially adaptive kernel learning, but also gives an explainable and intuitive understanding of what the model has learned which is often critically important for robotic tasks that interact with real-world environments.

Using all four datasets, the area under the curve (AUC) and mean negative log loss (MNLL) were calculated. As reported in Table 2, these metrics were also calculated for occupancy grid maps with dynamic updates (DOGM), variational sparse dynamic Gaussian process occupancy maps (VSDGPOM) (Senanayake et al., 2017), Hilbert Maps, and Bayesian Hilbert Maps with sequential updates (BHM). The best lengthscales for previous Hilbert mapping techniques were determined using five-fold cross-validation. For both RVI and IWVI version of ABHM, even when compared with hand-crafted features, ABHM outperforms. As extensions, we would like to allow inference on streaming data (McInerney et al., 2015) and explore a more diverse set of robot learning tasks such as pedestrian modeling (Jaipuria et al., 2018) and motion planning (Rana et al., 2017).

References

Christopher M Bishop. Pattern recognition and machine learning (information science and statistics), 1st edn. 2006. corr. 2nd printing edn. *Springer, New York*, 2007.

Yuri Burda, Roger Grosse, and Ruslan Salakhutdinov. Importance weighted autoencoders. *arXiv preprint arXiv:1509.00519*, 2015.

Kevin Doherty, Jinkun Wang, and Brendan Englot. Probabilistic map fusion for fast, incremental occupancy mapping with 3d hilbert maps. In *IEEE International Conference on Robotics and Automation (ICRA)*, pages 0–0, 2016.

James Hensman, Nicolo Fusi, and Neil D Lawrence. Gaussian processes for big data. *arXiv preprint arXiv:1309.6835*, 2013.

Tommi Jaakkola and Michael Jordan. A variational approach to bayesian logistic regression models and their extensions. In *Sixth International Workshop on Artificial Intelligence and Statistics (AISTATS)*, volume 82, 1997.

Nikita Jaipuria, Golnaz Habibi, and Jonathan P How. A transferable pedestrian motion prediction model for intersections with different geometries. *arXiv preprint arXiv:1806.09444*, 2018.

Diederik P Kingma and Max Welling. Auto-encoding variational bayes. *arXiv preprint arXiv:1312.6114*, 2013.

James McInerney, Rajesh Ranganath, and David Blei. The population posterior and bayesian modeling on streams. In *Advances in Neural Information Processing Systems*, 2015.

Daniel Meyer-Delius, Maximilian Beinhofer, and Wolfram Burgard. Occupancy Grid Models for Robot Mapping in Changing Environments. In *AAAI Conference on Artificial Intelligence (AAAI)*, 2012.

Andriy Mnih and Karol Gregor. Neural variational inference and learning in belief networks. *arXiv preprint arXiv:1402.0030*, 2014.

Radford M Neal. Probabilistic inference using markov chain monte carlo methods. 1993.

Christopher J Paciorek and Mark J Schervish. Nonstationary covariance functions for gaussian process regression. In *Advances in Neural Information Processing Systems (NIPS)*, pages 273–280, 2004.

John Paisley, David Blei, and Michael Jordan. Variational bayesian inference with stochastic search. *arXiv preprint arXiv:1206.6430*, 2012.

Fabio Ramos and Lionel Ott. Hilbert maps: scalable continuous occupancy mapping with stochastic gradient descent. In *Proceedings of Robotics: Science and Systems (RSS)*, Rome, Italy, July 2015.

Muhammad Asif Rana, Mustafa Mukadam, Seyed Reza Ahmadzadeh, Sonia Chernova, and Byron Boots. Towards robust skill generalization: Unifying learning from demonstration and motion planning. In *Conference on Robot Learning (CoRL)*, pages 109–118, 2017.

Rajesh Ranganath, Sean Gerrish, and David Blei. Black box variational inference. In *Artificial Intelligence and Statistics (AISTATS)*, pages 814–822, 2014.

Ransalu Senanayake and Fabio Ramos. Bayesian hilbert maps for dynamic continuous occupancy mapping. In *Conference on Robot Learning (CoRL)*, pages 458–471, 2017.

Ransalu Senanayake, Simon O'Callaghan, and Fabio Ramos. Learning highly dynamic environments with stochastic variational inference. In *IEEE International Conference on Robotics and Automation (ICRA)*, 2017.

Ransalu Senanayake, Anthony Tompkins, and Fabio Ramos. Automorphing kernels for nonstationarity in mapping unstructured environments. 2018.

Cyrill Stachniss and Wolfram Burgard. Mobile robot mapping and localization in non-static environments. In *AAAI Conference on Artificial Intelligence (AAAI)*, pages 1324–1329, 2005.

Dustin Tran, Matthew D. Hoffman, Rif A. Saurous, Eugene Brevdo, Kevin Murphy, and David M. Blei. Deep probabilistic programming. In *International Conference on Learning Representations (ICLR)*, 2017.

Appendix A. Introduction

Figure 3 shows the importance of modeling the nonstationarity (Paciorek and Schervish, 2004) to capture abrupt changes in response variables. This is extremely important for robotic mapping as sharp edges are ubiquitous in real world environments.

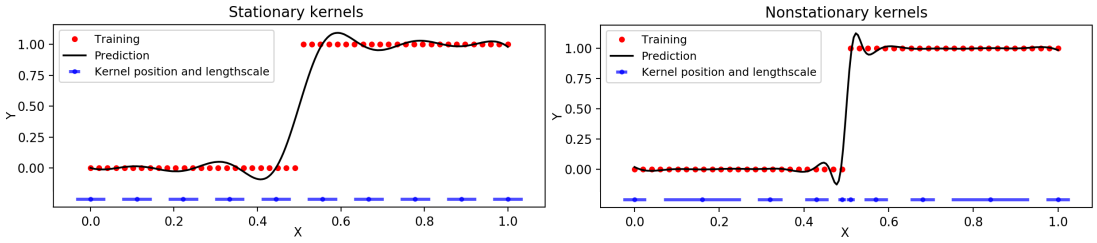

Figure 3: Comparison of stationary and nonstationary squared-exponential kernels, $\exp(-\|\mathbf{x} - \tilde{\mathbf{x}}\|_2^2/2l^2)$ with bivariate Gaussian distributions $\tilde{\mathbf{x}}$ hinged on the environment with lengthscales l, and their ability to represent sharp spatial changes. Note that both examples have the same number of kernels, however in the non-stationary case the kernels have different positions and lengthscales to account for abrupt changes in the training data.

Appendix B. Model

Since observed occupancy values are always binary and they are independent of each other, we assume the likelihood follows a Bernoulli distribution $p(\mathbf{y}|\mathbf{x}, \mathbf{w}, \mathbf{l}, \tilde{\mathbf{x}})$ where $\log(\theta/(1-\theta))) = \mathbf{w}^\top \Phi(\mathbf{x}; \mathbf{l}, \tilde{\mathbf{x}})$. The prior distributions over weights are defined as Gaussian distributions. Since the hinge locations can be anywhere in the space, they are also defined as Normal distributions. As shown in Figure 4, kernel functions are now implicitly evaluated between datapoints point and hinge distributions, naturally accounting for uncertainty. A meaningful lengthscale can only be positive and hence the prior distribution over inverse squared-lengthscales $\bar{l} = 1/2l^2$ is defined as a gamma distribution. The first three rows of Table 1 provides a summary of all variables. Here, for computational efficiency we assume all variables are independent. As these prior distributions were empirically sufficient for modeling occupancy, we do not complicate the model with hyper-prior distributions.

The gamma distribution is defined as $\mathcal{G}(x; \alpha, \beta) := \frac{\beta^\alpha}{\Gamma(\alpha)} x^{\alpha-1} e^{-\beta x}$ where $\Gamma(\alpha) := \int_0^\infty z^{\alpha-1} e^{-z} \mathrm{d}z$ is the gamma function. $\alpha > 0$ is the shape parameter and $\beta > 0$ is the rate parameter. In literature, the scale parameter is sometimes defined as the inverse of the rate parameter instead of the rate parameter. The log-normal distribution $\mathcal{LN}$ is obtained by transforming a standard normal variable $z' = \exp(\mu + \sigma z)$. To keep variances of variational distributions non-negative a softplus transformation was applied.

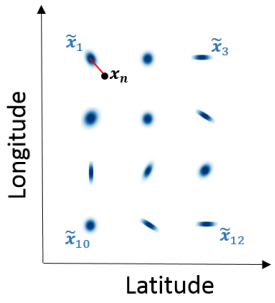

Figure 4: Feature vector computation. $\{\tilde{\mathbf{x}}\}_{m=1}^{M=12}$ are hinge distributions and $\mathbf{x}_n$ is the n^{th} data point.

Appendix C. Experiments

All experiments were conducted on a computer with a GTX1080 Ti 11 GB. On average it takes around 10 minutes to learn upwards of 57,600 parameters (8 parameters per hinge with more than 7200 hinges) and 300,000 data points. In contrast, Senanayake and Ramos (2017) has an inevitable computational complexity $\mathcal{O}(M^3)$ while the proposed method uses stochastic gradient descent (SGD). Although analyzing the theoretical asymptotic complexity is not straightforward, it linearly increases with M and N empirically. In ABHM, we take the advantage of SGD to scale for large datasets. Descriptions of the datasets can be found in Senanayake et al. (2018).

Table 3: Description of the datasets.

Dataset	Real	Dynamic	Description
1	✗	✗	A 600×300 m^2 area. This is a simple but large environment.
2	✓	✗	Intel lab dataset: a complex indoor environment.
3	✗	✓	Vehicles move in two directions and the robot sits in the middle.
4	✓	✓	Lidar dataset in a busy intersection.